DINAME 2019 - Proceedings of the XVIII International Symposium on Dynamic Problems of Mechanics,
M.A. Savi, T.G. Ritto and W.M. Bessa (Editors), ABCM, Buzios, RJ, Brazil, March 10th to 15th, 2019

Attitude and vibration control of satellites featuring flexible panels combining reaction wheels and viscoelastic materials

Lewton M. Rodrigues[1], **Domingos A. Rade**[1], **Thiago de P. Sales**[1] **and Ijar M. da Fonseca**[1]

[1] Mechanical Engineering Division, ITA-DCTA, São José dos Campos, Brazil

Abstract: It is widely known that elastic vibrations of highly flexible appendages, such as solar panels, can jeopardize the pointing accuracy of spacecraft, which can be subjected to very strict requirements in a number of practical situations. In this context, this work addresses the attitude and vibration control of artificial satellites featuring flexible solar panels, by combining reaction wheels for attitude control and viscoelastic materials for the attenuation of elastic vibrations of the panels. First, a high-fidelity three-dimensional finite element model, developed for the flexible parts of the satellite, is presented. The model accounts for the presence of viscoelastic dampers in the form of springs used for interconnecting the segments of the panels. The viscoelastic behavior is modeled by using a constitutive model based on derivatives of fractional order, which is convenient for both frequency- and time-domain simulations. The finite element model is associated with rigid-body equations of motion, which enable determination of the attitude motion of the satellite in terms of Euler's angles. Numerical simulations are performed considering an orbital station-keeping correction maneuver driven by the use of thrusters, with attitude control being performed by reaction wheels, which are commanded by a proportional-integral-derivative feedback law. By comparing transient results, one shows that viscoelastic dampers are effective in providing faster reduction of vibration levels of the satellite panels, and minimization of attitude perturbations.

Keywords: attitude control, vibration control, viscoelastic damping, flexible spacecraft

INTRODUCTION

Since the beginning of space-related activities, flexible appendages such as antennas and solar panels used for data transmission and power supply have been incorporated into spacecraft. Due to the typically low damping levels that spacecraft are subjected to in space, maneuvers such as attitude correction can induce vibrations in the flexible parts. Consequently, the interaction between the rigid body motion and the flexibility can induce disturbances in the system attitude (Modi, 1974). These disturbances can be harmful if a spacecraft is required to have strict precision requirements. A sound example is the Hubble space telescope, which must fulfill extremely high pointing-accuracy requirements.

For this reason, it is necessary to have a vibration control system that can alleviate these disturbances and keeping the objective of operation of the satellite. Several control techniques have been proposed with the aim of reducing excitation or accelerating the decay of the flexible appendage oscillations, especially during attitude maneuvers. Among the active control techniques, some of the strategies reported in the literature are: the use of optical measurements combined with an actuator for vibration suppression in flexible spacecraft (Wang *et al.*, 2016); the use of variable-structure control based on a sliding surface (Bang *et al.*, 2005); predictive control based on Genetic Algorithm (TayyebTaher and Esmaeilzadeh, 2017). On the other hand, authors of the present work investigated a passive control strategy consisting in the use of piezoelectric transducers attached to the flexible parts of a spacecraft connected to electric circuit in order to reduce oscillations by transforming vibratory energy into electric energy (Sales *et al.*, 2013).

Viscoelastic materials, frequently presented in the form of rubber-like elastomers, have long been used for vibration attenuation in various types of mechanical systems (civil engineering structures, ground and aerospace vehicles, industrial equipment, etc). As a further application of viscoelastic materials, the main objective of this paper is to investigate the possibility of improvement in the performance of combined attitude and vibration control of spacecraft containing flexible solar array generators (SAGs), by associating reaction wheels (RWs) for attitude control and viscoelastic materials for the attenuation of flexible motion.

To achieve the aforementioned objective, a three-dimensional finite element (FE) model is initially developed for the flexible parts of the satellite. The model accounts for the presence of viscoelastic dampers in the form of springs interconnecting the segments of the SAGs' panels. The viscoelastic behavior is taken into account by using a constitutive model based on derivatives of fractional order, which is convenient for both frequency- and time-domain simulations. The FE model is then associated with the rigid-body equations of motion, which enable prediction of the attitude motion of the satellite in terms of Euler's angles. For an orbital station-keeping correction maneuver driven by a thruster command, numerical simulations are performed to investigate the benefits that the use of viscoelastic dampers can provide in terms of reduction of vibration levels of the spacecraft SAGs, and minimization of attitude perturbations. The attitude control subsystem (ACS) comprises RWs which are commanded through proportional-integral-derivative feedback. Based on

obtained results, conclusions are finally drawn on the advantages and shortcomings of the suggested control strategy.

SYSTEM DESCRIPTION

The satellite considered in this work resembles the Brazilian Amazonia-1 (see Fig. 1). The satellite consists of a rigid hub with two flexible SAGs. Each SAG contains three interconnected plate-like segments, one of which is attached to the hub through a yoke. Plates are connected to each other and to the yoke by spring-like elements.

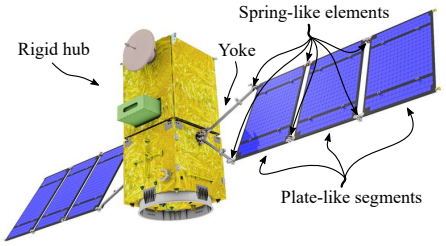

Figure 1: Brazilian Amazonia-1 satellite

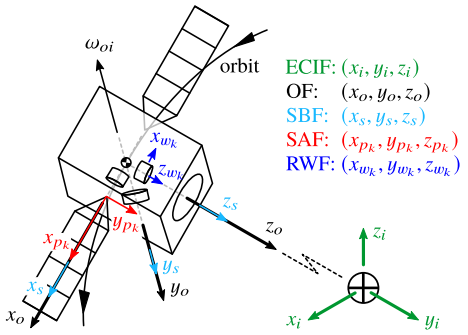

Figure 2: Reference frames

EQUATIONS OF MOTION

Initially, five reference frames are defined, as shown in Fig. 2: the Earth centered inertial frame (ECIF); the orbital frame (OF); the spacecraft-hub body frame (SBF); frames attached to the reaction wheels (RWFs); and solar panels' frames (SPFs). Then, by making use of Lagrangian mechanics, one can obtain the equations of motion for the spacecraft considered in this work. One highlights that the satellite has a rigid hub; $N_w = 3$ RWs; and $N_p = 2$ SAGs, which are taken as being flexible structures, and discretized using FEs. It can be shown that:

$$
\begin{aligned}
&M_s\,\ddot{\mathbf{r}}_h + \mathbf{T}_{is}\,\mathscr{C}_{\mathbf{r}_h\theta_{is}}\,\bar{\mathbf{G}}\,\ddot{\theta}_{is} + \mathbf{T}_{is}\,\dot{\mathscr{C}}_{\mathbf{r}_h\theta_{is}}\,\bar{\mathbf{G}}\,\dot{\theta}_{is} + \mathbf{T}_{is}\left(\bar{\mathbf{G}}\,\dot{\theta}_{is}\right)^{\times}\mathscr{C}_{\mathbf{r}_h\theta_{is}}\,\bar{\mathbf{G}}\,\dot{\theta}_{is} + \mathbf{T}_{is}\sum_{k=1}^{N_p}\mathbf{T}_{sp_k}\,\bar{\mathbf{S}}\,\ddot{\bar{\mathbf{r}}}_{p_k} \\
&\quad + \mathbf{T}_{is}\left(\bar{\mathbf{G}}\,\dot{\theta}_{is}\right)^{\times}\sum_{k=1}^{N_p}\mathbf{T}_{sp_k}\,\bar{\mathbf{S}}\,\dot{\bar{\mathbf{r}}}_{p_k} + \mathbf{T}_{is}\sum_{k=1}^{N_p}\mathbf{T}_{sp_k}\,\bar{\boldsymbol{\omega}}^{\times}_{sp_k}\,\bar{\mathbf{S}}\,\dot{\bar{\mathbf{r}}}_{p_k} - \mathbf{T}_{is}\sum_{k=1}^{N_p}\mathbf{T}_{sp_k}\,\bar{\mathbf{R}}^{\times}_{p_k}\,\dot{\bar{\boldsymbol{\omega}}}_{sp_k} \\
&\quad - \mathbf{T}_{is}\left(\bar{\mathbf{G}}\,\dot{\theta}_{is}\right)^{\times}\sum_{k=1}^{N_p}\mathbf{T}_{sp_k}\,\bar{\mathbf{R}}^{\times}_{p_k}\,\bar{\boldsymbol{\omega}}_{sp_k} - \mathbf{T}_{is}\sum_{k=1}^{N_p}\mathbf{T}_{sp_k}\left[\bar{\boldsymbol{\omega}}^{\times}_{sp_k}\,\bar{\mathbf{R}}^{\times}_{p_k} + \left(\bar{\mathbf{S}}\,\dot{\bar{\mathbf{r}}}_{p_k}\right)^{\times}\right]\bar{\boldsymbol{\omega}}_{sp_k} = \mathbf{F}_g = -\frac{\mu M_s}{\|\mathbf{r}_h\|^3}\mathbf{r}_h\,; \qquad (1)
\end{aligned}
$$

$$
\begin{aligned}
&\bar{\mathbf{G}}^{\mathrm{T}}\mathbf{J}_s\,\bar{\mathbf{G}}\,\ddot{\theta}_{is} + 2\,\dot{\bar{\mathbf{G}}}^{\mathrm{T}}\mathbf{J}_s\,\bar{\mathbf{G}}\,\dot{\theta}_{is} + \bar{\mathbf{G}}^{\mathrm{T}}\dot{\mathbf{J}}_s\,\bar{\mathbf{G}}\,\dot{\theta}_{is} + \bar{\mathbf{G}}^{\mathrm{T}}\sum_{k=1}^{N_w}\mathbf{T}_{sw_k}\,\mathbf{J}_{w_k}\,\bar{\mathbf{G}}_{sw_k}\,\ddot{\theta}_{sw_k} + 2\,\dot{\bar{\mathbf{G}}}^{\mathrm{T}}\sum_{k=1}^{N_w}\mathbf{T}_{sw_k}\,\mathbf{J}_{w_k}\,\bar{\mathbf{G}}_{sw_k}\,\dot{\theta}_{sw_k} \\
&\quad + \bar{\mathbf{G}}^{\mathrm{T}}\sum_{k=1}^{N_w}\mathbf{T}_{sw_k}\,\bar{\boldsymbol{\omega}}^{\times}_{sw_k}\,\mathbf{J}_{w_k}\,\bar{\mathbf{G}}_{sw_k}\,\dot{\theta}_{sw_k} + \bar{\mathbf{G}}^{\mathrm{T}}\mathscr{C}^{\mathrm{T}}_{\mathbf{r}_h\theta_{is}}\,\mathbf{T}^{\mathrm{T}}_{is}\,\ddot{\mathbf{r}}_h + 2\,\dot{\bar{\mathbf{G}}}^{\mathrm{T}}\mathscr{C}^{\mathrm{T}}_{\mathbf{r}_h\theta_{is}}\,\mathbf{T}^{\mathrm{T}}_{is}\,\dot{\mathbf{r}}_h + \bar{\mathbf{G}}^{\mathrm{T}}\mathscr{C}^{\mathrm{T}}_{\mathbf{r}_h\theta_{is}}\left(\mathbf{T}^{\mathrm{T}}_{is}\,\dot{\mathbf{r}}^{\times}_h\,\mathbf{T}_{is}\right)\bar{\mathbf{G}}\,\dot{\theta}_{is} \\
&\quad - \bar{\mathbf{G}}^{\mathrm{T}}\left(\mathbf{T}^{\mathrm{T}}_{is}\,\dot{\mathbf{r}}^{\times}_h\,\mathbf{T}_{is}\right)\mathscr{C}^{\mathrm{T}}_{\mathbf{r}_h\theta_{is}}\,\bar{\mathbf{G}}\,\dot{\theta}_{is} + \bar{\mathbf{G}}^{\mathrm{T}}\sum_{k=1}^{N_p}\mathscr{C}^{\mathrm{T}}_{\mathbf{r}_{p_k}\theta_{is}}\,\ddot{\bar{\mathbf{r}}}_{p_k} + 2\,\dot{\bar{\mathbf{G}}}^{\mathrm{T}}\sum_{k=1}^{N_p}\mathscr{C}^{\mathrm{T}}_{\mathbf{r}_{p_k}\theta_{is}}\,\dot{\bar{\mathbf{r}}}_{p_k} + \bar{\mathbf{G}}^{\mathrm{T}}\sum_{k=1}^{N_p}\dot{\mathscr{C}}^{\mathrm{T}}_{\mathbf{r}_{p_k}\theta_{is}}\,\dot{\bar{\mathbf{r}}}_{p_k} \\
&\quad + \bar{\mathbf{G}}^{\mathrm{T}}\sum_{k=1}^{N_p}\mathscr{C}^{\mathrm{T}}_{\bar{\boldsymbol{\omega}}_{sp_k}\theta_{is}}\,\dot{\bar{\boldsymbol{\omega}}}_{sp_k} + 2\,\dot{\bar{\mathbf{G}}}^{\mathrm{T}}\sum_{k=1}^{N_p}\mathscr{C}^{\mathrm{T}}_{\bar{\boldsymbol{\omega}}_{sp_k}\theta_{is}}\,\bar{\boldsymbol{\omega}}_{sp_k} + \bar{\mathbf{G}}^{\mathrm{T}}\sum_{k=1}^{N_p}\dot{\mathscr{C}}^{\mathrm{T}}_{\bar{\boldsymbol{\omega}}_{sp_k}\theta_{is}}\,\bar{\boldsymbol{\omega}}_{sp_k} + 2\theta_{is}\lambda \\
&\quad = \bar{\mathbf{G}}^{\mathrm{T}}\mathbf{T}_g + \bar{\mathbf{G}}^{\mathrm{T}}\mathbf{T}_m = \bar{\mathbf{G}}^{\mathrm{T}}\frac{3\mu}{\|\mathbf{r}_h\|^5}\left(\mathbf{T}^{\mathrm{T}}_{is}\,\mathbf{r}_h\right)^{\times}\mathbf{J}_s\,\mathbf{T}^{\mathrm{T}}_{is}\,\mathbf{r}_h + \bar{\mathbf{G}}^{\mathrm{T}}\,\mathbf{m}^{\times}\,\mathbf{T}^{\mathrm{T}}_{is}\,\mathbf{B}_{\oplus}\,; \qquad (2)
\end{aligned}
$$

$$
\begin{aligned}
&\bar{\mathbf{G}}^{\mathrm{T}}_{sw_k}\,\mathbf{J}_{w_k}\,\mathbf{T}^{\mathrm{T}}_{sw_k}\,\bar{\mathbf{G}}\,\ddot{\theta}_{is} + \bar{\mathbf{G}}^{\mathrm{T}}_{sw_k}\,\mathbf{J}_{w_k}\,\bar{\mathbf{G}}_{sw_k}\,\ddot{\theta}_{sw_k} + \bar{\mathbf{G}}^{\mathrm{T}}_{sw_k}\left[\mathbf{J}_{w_k}\,\mathbf{T}^{\mathrm{T}}_{sw_k}\left(\bar{\mathbf{G}}\,\dot{\theta}_{is}\right)^{\times}\mathbf{T}_{sw_k} + \mathbf{T}^{\mathrm{T}}_{sw_k}\left(\bar{\mathbf{G}}\,\dot{\theta}_{is}\right)^{\times}\mathbf{T}_{sw_k}\,\mathbf{J}_{w_k}\right]\bar{\mathbf{G}}_{sw_k}\,\dot{\theta}_{sw_k} \\
&\quad + \bar{\mathbf{G}}^{\mathrm{T}}_{sw_k}\,\mathbf{T}^{\mathrm{T}}_{sw_k}\left(\bar{\mathbf{G}}\,\dot{\theta}_{is}\right)^{\times}\mathbf{T}_{sw_k}\,\mathbf{J}_{w_k}\,\mathbf{T}^{\mathrm{T}}_{sw_k}\,\bar{\mathbf{G}}\,\dot{\theta}_{is} = T_{c,w_k}\,; \qquad (3)
\end{aligned}
$$

$$
\begin{aligned}
&\mathbf{M}_{p_k}\,\ddot{\bar{\mathbf{r}}}_{p_k} + \bar{\mathbf{S}}^{\mathrm{T}}\,\mathbf{T}^{\mathrm{T}}_{sp_k}\,\mathbf{T}^{\mathrm{T}}_{is}\,\ddot{\mathbf{r}}_h + \mathscr{C}_{\mathbf{r}_{p_k}\theta_{is}}\,\bar{\mathbf{G}}\,\ddot{\theta}_{is} - \left\{\bar{\mathbf{S}}^{\mathrm{T}}\,\mathbf{T}^{\mathrm{T}}_{sp_k}\left(\bar{\mathbf{G}}\,\dot{\theta}_{is}\right)^{\times}\mathbf{r}^{\times}_{a_k} + \left[\left(\bar{\boldsymbol{\omega}}^{\mathrm{T}}_{sp_k}\,\frac{\partial\mathbf{J}_{p_k}}{\partial\bar{\mathbf{r}}_{p_k}}\right) + \bar{\mathbf{S}}^{\mathrm{T}}\,\bar{\boldsymbol{\omega}}^{\times}_{sp_k}\right.\right. \\
&\quad \left.\left. + \frac{1}{2}\,\dot{\theta}^{\mathrm{T}}_{is}\,\bar{\mathbf{G}}^{\mathrm{T}}\,\mathbf{T}_{sp_k}\,\frac{\partial\mathbf{J}_{p_k}}{\partial\bar{\mathbf{r}}_{p_k}}\right]\mathbf{T}^{\mathrm{T}}_{sp_k}\right\}\bar{\mathbf{G}}\,\dot{\theta}_{is} + \bar{\mathbf{S}}^{\mathrm{T}}\,\dot{\bar{\boldsymbol{\omega}}}_{sp_k} - \frac{1}{2}\,\bar{\boldsymbol{\omega}}^{\mathrm{T}}_{sp_k}\,\frac{\partial\mathbf{J}_{p_k}}{\partial\bar{\mathbf{r}}_{p_k}}\,\frac{\partial\mathbf{J}_{p_k}}{\partial\bar{\mathbf{r}}_{p_k}}\,\bar{\boldsymbol{\omega}}_{sp_k} + \left[\mathbf{K}_{p_k} + c^{(v)}\left(\frac{G^{(v)}_{\infty} - G^{(v)}_0}{G^{(v)}_0}\right)\mathbf{K}^{(v)}_{p_k}\right]\bar{\mathbf{r}}_{p_k} \\
&\quad = -\bar{\mathbf{S}}^{\mathrm{T}}\,\mathbf{T}^{\mathrm{T}}_{sp_k}\,\mathbf{T}^{\mathrm{T}}_{is}\,\frac{\mu}{\|\mathbf{r}_h\|^3}\mathbf{r}_h - c^{(v)}\frac{G^{(v)}_{\infty}}{G^{(v)}_0}\mathbf{K}^{(v)}_{p_k}\sum_{j=1}^{N_t}A_j\left(\bar{\boldsymbol{r}}_{p_k}\right)_{t_{n+1-j}} \qquad (4)
\end{aligned}
$$

are the equations of motion related to the translation of the center of mass (CoM) of the rigid hub, the spacecraft attitude w.r.t. the ECIF, the k-th RW angular coordinate, and the k-th SAG FE model degrees-of-freedom (DoFs), respectively. The position vector of the rigid hub CoM with respect to ECIF is denoted by $\mathbf{r}_h$; $\bar{\mathbf{r}}_{p_k}$ is the vector of global FE DoFs of

the k-th SAG; θ_{is} is a vector whose components are Euler parameters, used to describe the attitude of the SBF w.r.t. the ECIF; θ_{sw_k} is the spin angle of the k-th RWF w.r.t. the SBF; $\bar{\boldsymbol{\omega}}_{sp_k}$ is the angular velocity of the k-th SAG w.r.t. the SBF, which is assumed as being known. Furthermore, $\mathbf{T}_{is}$ is the rotation matrix used to change basis from the SBF to the ECIF; $\mathbf{T}_{sw_k}$ transforms vector coordinates from the k-th RWF to the SBF; and $\mathbf{T}_{sp_k}$ changes basis from the k-th SPF to the SBF. External loads include the gravitational force $\mathbf{F}_g$, the gravity gradient torque $\mathbf{T}_g$, and the geomagnetic torque $\mathbf{T}_m$. The total mass and the inertia tensor of the satellite, which incorporates flexible motion contributions, are indicated respectively by M_s and $\mathbf{J}_s$. $\mathbf{M}_{p_k}$ and $\mathbf{K}_{p_k}$ are the mass and stiffness matrices associated with the k-th SAG, respectively. $\mathbf{K}_{p_k}^{(v)}$ is the stiffness matrix associated with the viscoelastic elements on the system; it is computed assuming elastic behavior. One also has $\mathbf{K}_{p_k} = \mathbf{K}_{p_k}^{(el)} + \mathbf{K}_{p_k}^{(v)}$, where $\mathbf{K}_{p_k}^{(el)}$ stands for the stiffness matrix of the linear elastic portions of the spacecraft system. The viscoelastic behavior is modeled in Eq. (4) using fractional derivative constitutive equations, following the procedures outlined by Galucio *et al.* (2004). $G_0^{(v)}$ and $G_\infty^{(v)}$ are, respectively, the relaxed and the non-relaxed transversal elastic moduli, whereas $c^{(v)}$ stands for a constant depending on the integration time step, as well as on the relaxation time constant $\tau^{(v)}$ and on the fractional order $\alpha^{(v)}$, both of which are viscoelastic material properties. The former four model parameters can be calculated, for instance, using empirical curves and equations given by Soovere and Drake (1985), for a given material. The last term on the right-hand side of Eq. (4) accounts for the memory effect of the viscoelastic material, $\bar{\boldsymbol{r}}_{p_k}$ being a vector of internal variables of the constitutive model. Finally, it is noticed that a Lagrange multiplier λ is used to ensure independence among the components of θ_{is}. For this reason, equations of motion are augmented with the constraint equation $C = \theta_{is}^{\mathrm{T}}\theta_{is} - 1 = 0$, which is stabilized within the solution procedures using the Baumgarte method. The work of da Fonseca *et al.* (2017) can be consulted for greater details concerning other parameters, and developments.

NUMERICAL SIMULATIONS

Physical properties of the system

All the simulations were performed using the spacecraft orbit data presented in Tab. 1. The rigid hub has dimensions of 2.0 m × 2.2 m × 1.8 m; mass $M_h = 500$ kg; and inertia tensor equal to:

$$\mathbf{J}_h = \begin{bmatrix} 226.90 & -0.50 & -3.67 \\ -0.50 & 261.42 & 2.70 \\ -3.67 & 2.70 & 76.98 \end{bmatrix} \text{kg·m}^2 . \tag{5}$$

The RWs are considered to have an inertia moment equal to 0.0302 kg·m^2 around their spin axis. While no constraints have been enforced for their maximum control torque, angular speeds have been limited to 6000 RPM.

Structural finite element model for the solar array generators

To create the FE model for the SAGs, the ANSYS® software was used. This model, shown in Fig. 3, comprises a total of 1404 SHELL181 elements for the three distinct panels; 408 BEAM188 elements for the yoke and the frames of the panels; and 6 COMBIN14 elements for torsional springs used to connect distinct panels and one of them to the yoke, cf. Fig. 1. The materials of the SAG panels and yoke are assumed to show linear elastic behavior. The properties adopted for the material of the SAG panels were: $E = 5$ GPa, $\nu = 0.33$, $\rho = 140.8$ kg·m^{-3}. Whereas, for the yoke: $E = 50$ GPa, $\nu = 0.33$, $\rho = 2160$ kg·m^{-3}. The thickness of the SAG panels is 22 mm. The yoke and frames have a square cross-section with sides equal to 22 mm. The yoke of each SAG is assumed to be clamped to the rigid hub of the satellite.

Mass and stiffness matrices were extracted from ANSYS® and then imported into MATLAB®. Viscoelastic material behavior was initially incorporated into the model using frequency- and temperature-dependent complex stiffness for the torsional springs of the COMBIN14 FEs. The first dynamic analysis that was performed involved computation of the natural frequencies and mode shapes of an isolated SAG, which are shown in Fig. 4. Structural damping was later incorporated by assuming modal damping factors equal to 0.5% for all vibration modes.

Table 1: Spacecraft orbit data

Epoch		Nov 09, 2018, 05:30:13 UTC
Eccentricity	e	0.0001072
Semi-major axis	a	715.1137 km
Inclination	i	98.4003°
RAAN*	Ω	0.3692°
Perigee argument	ω	0.9863°
Mean anomaly	M	0.5299°

*Right ascension of the ascending node

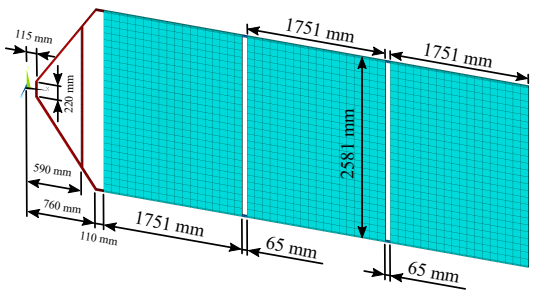

Figure 3: SAG dimensions and FE discretization

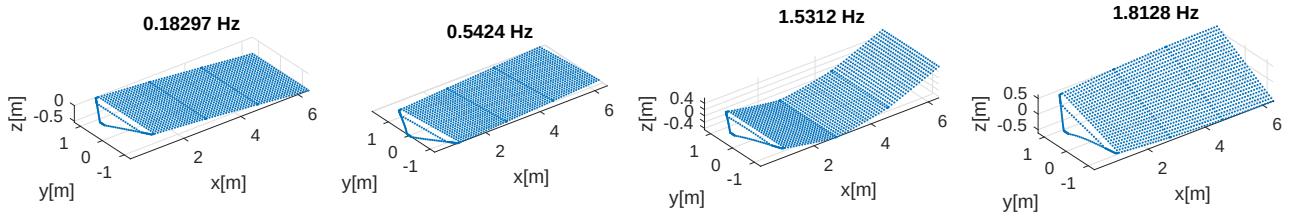

Figure 4: First four solar array generator mode shapes

Selection of a suitable material for the viscoelastic torsional springs/dampers

The material used in the viscoelastic torsional springs/dampers was selected to be the 3M^{TM} Acrylic Foam 18. It was chosen because of its high loss factor values in low frequencies, and within the operational temperature range of the spacecraft (−50°C to 50°C). This implies in a superior capability to mitigate vibration in comparison with other materials, which show smaller loss factor values. In this regard, the report of Soovere and Drake (1985) can be used as a guideline as it gathers experimental data for many viscoelastic materials.

Model order reduction through modal truncation

Owed to the fact that the SAGs FE model has a large number of DoFs, its modal basis was truncated and used to perform model order reduction, and thus alleviate computational simulation costs. Still, the most relevant characteristics of the SAGs dynamic behavior were retained from the complete model.

Attitude control subsystem

As discussed previously, RWs have been considered for controlling the attitude of the spacecraft. Electric motors are responsible for providing PID feedback torques to the RWs. They are evaluated according to:

$$\begin{bmatrix} T_{c,w_1} & T_{c,w_2} & T_{c,w_3} \end{bmatrix}^{\mathrm{T}} = K_P\, \boldsymbol{\theta}_{error}/\theta_{error}^3 + K_I \int_0^t \boldsymbol{\theta}_{error}\, d\tau + K_D\, \bar{\mathbf{G}} \left(\dot{\Theta}_{is} - \dot{\Theta}_{is_d} \right) \tag{6}$$

where Θ_{is_d} contains the desired Euler parameters, and $\Theta_{error} = \begin{bmatrix} \theta_{error} & \boldsymbol{\theta}_{error}^{\mathrm{T}} \end{bmatrix}^{\mathrm{T}}$, with:

$$\Theta_{error} = \begin{bmatrix} \theta_{is_d} & \boldsymbol{\theta}_{is_d}^{\mathrm{T}} \\ \boldsymbol{\theta}_{is_d} & \theta_{is_d}\mathbf{I}_3 - \boldsymbol{\theta}_{is_d}^{\times} \end{bmatrix} \Theta_{is}\,, \tag{7}$$

being $\Theta_{is_d} = \begin{bmatrix} \theta_{is,d} & \boldsymbol{\theta}_{is,d}^{\mathrm{T}} \end{bmatrix}^{\mathrm{T}}$. K_P, K_I and K_D are the gains of the PID controller, which were determined using the Ziegler–Nichols procedure. For the analyzed system, one arrived at $K_P = 4780$, $K_I = 3.5941$, and $K_D = 7705.5$.

Simulation procedures

The equations of motion of the spacecraft system were numerically integrated in time. For this purpose, due to nonlinear behavior, a composite implicit integrator was considered (Bathe and Baig, 2005). Resulting nonlinear algebraic equations were numerically solved using the `fsolve` routine available in the MATLAB® software. The selected time step increment was at least 50 times smaller than the smallest natural period among the retained flexible modes, for accuracy considerations.

RESULTS

Two distinct cases have been simulated to assess the attitude control performed by the RWs, as well as the control of elastic vibratory motions by the viscoelastic springs/dampers. In both cases, the satellite was considered to be orbiting Earth undisturbed. A rectangular pulse force was applied by a thruster, to simulate an orbital station-keeping maneuver. This load aims to provide a budget of $\Delta v = 0.5$ m/s in $\Delta t = 1$ s, without generating any torque in the spacecraft. While in the first case the satellite is taken as being symmetric, with the two SAGs being aligned w.r.t. each other and the SBF; in the second case, one of the SAGs exhibits an angular rotation misalignment of 1° w.r.t. its counterpart and the SBF. To simulate the viscoelastic material constitutive behavior, temperature was taken equal to 27°C.

Case 1

Figures 5–7 show the influence exerted by the viscoelastic spring/dampers in the attitude control efforts and elastic vibration responses. These figures show, respectively, the time histories of the modal coordinates associated with one of the flexible SAGs; the control torques demanded from the RWs; and the transverse elastic displacement of the free tip of a SAG. The plots given in Fig. 5 clearly show that the modal coordinates $(\mathbf{q}_{p_1})_1$, $(\mathbf{q}_{p_1})_2$ and $(\mathbf{q}_{p_1})_3$ have a faster decay rate when viscoelastic springs/dampers are added to the system. Results provided in Fig. 6 also indicate that the PID

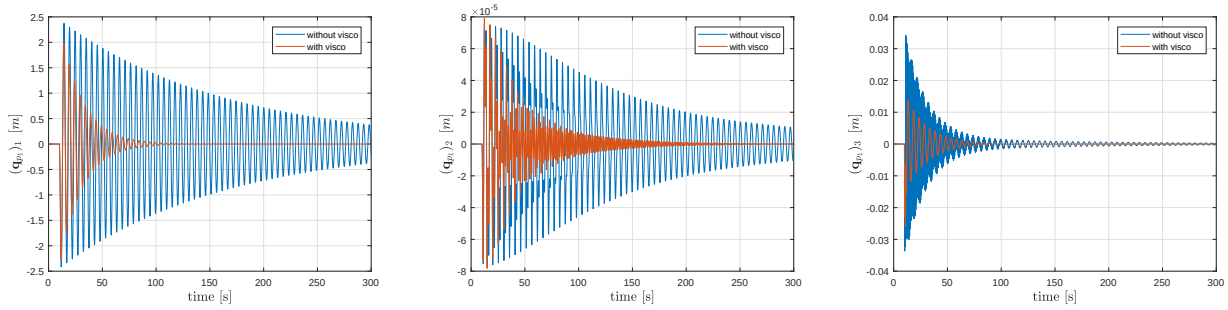

Figure 5: Time histories of the modal coordinates of one of the SAGs for the first simulation scenario

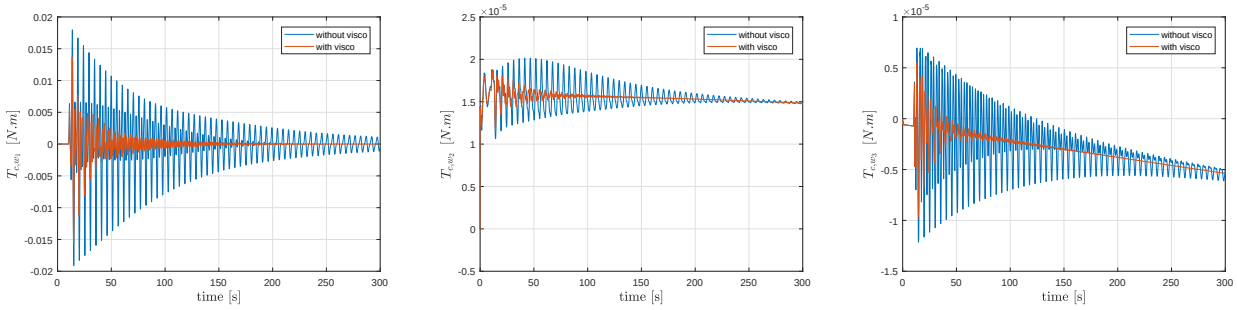

Figure 6: Control torques demanded from each RW in the first simulation scenario

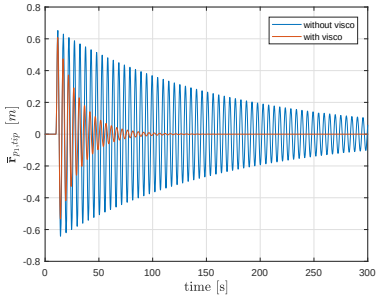

Figure 7: Transversal displacement of the tip of one of the SAGs in the first simulation scenario

control torques have smaller magnitudes thanks to the addition of viscoelastic springs/dampers to the system. Likewise, the transverse displacement of the tip of one of the SAGs, shown in Fig. 7, displays a faster decay rate when viscoelastic damping is incorporated for the control of elastic, vibratory motions. All these results point to the fact that viscoelastic damping can, indeed, effectively attenuate flexible motions of spacecraft, and also significantly reduce control efforts of the satellite ACS, in strikingly shorter intervals of time. Nevertheless, the thruster excitation did not influence the spacecraft attitude responses, since the two SAGs deformed elastically in phase w.r.t. each other, which balances out flexibility perturbations in the spacecraft attitude.

Case 2

As seen in the first simulation scenario, the spacecraft attitude was not disturbed by the thruster action due to the occurrence of symmetric vibrations of the SAGs. In the alternative case considered now, the system was simulated with one of the SAGs having an angular deviation of 1° w.r.t. its counterpart. Results are presented in Figs. 8–11. As observed

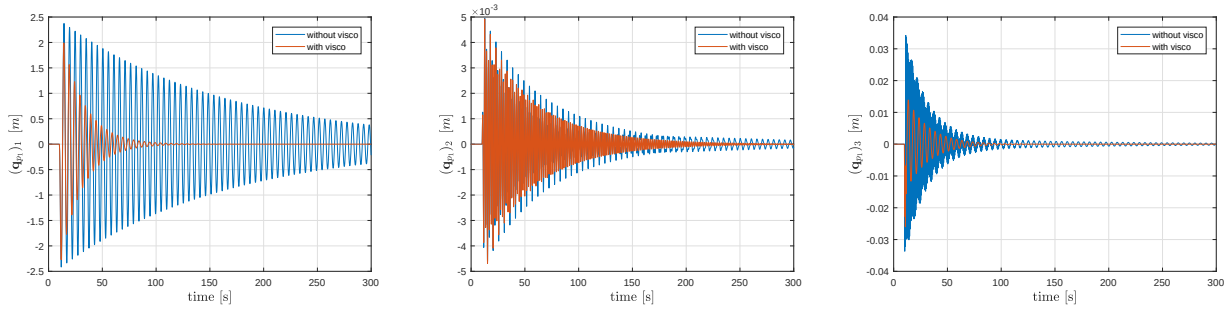

Figure 8: Time histories of the modal coordinates of one of the SAGs for the second simulation scenario

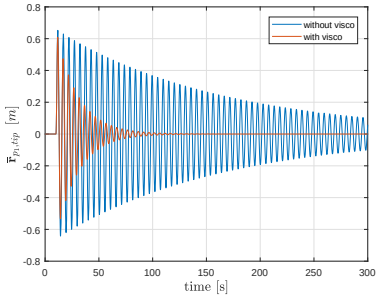

Figure 9: Transversal displacement of the tip of a SAG in the second simulation scenario

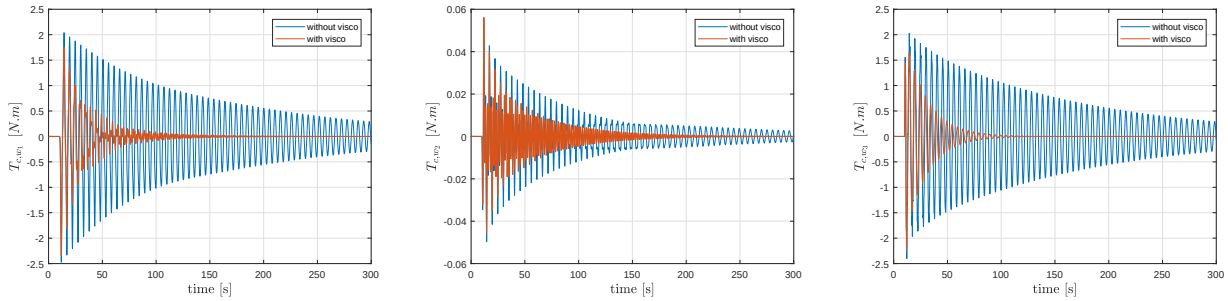

Figure 10: Control torques demanded from each RW in the second simulation scenario

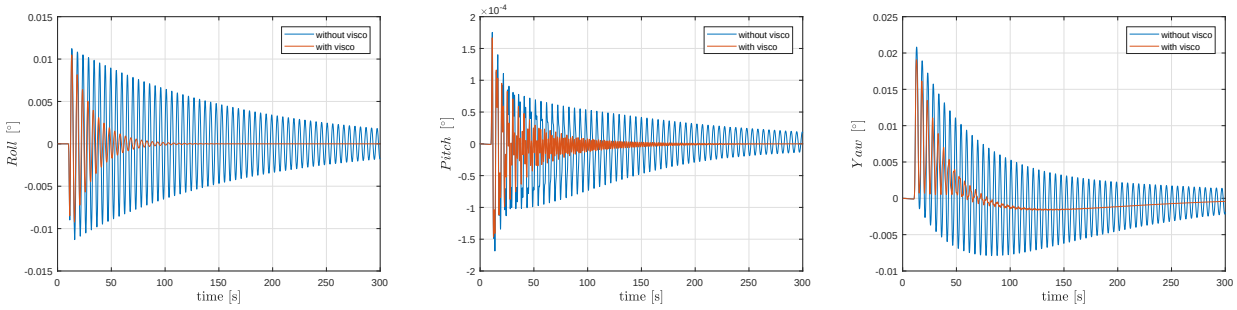

Figure 11: Deviations in the attitude Euler angles in the second simulation scenario

previously for the first analyzed case, modal coordinates $(\mathbf{q}_{p_1})_1$, $(\mathbf{q}_{p_1})_2$ and $(\mathbf{q}_{p_1})_3$ are largely attenuated when viscoelastic damping is included in the system.

Figure 10 shows that the control torques required by the RWs have larger magnitudes for the second case, in comparison with the first one. Figure 11 readily shows that, now, the attitude angles are disturbed by the simulated orbital station-keeping maneuver. This is a direct consequence of the slight asymmetric arrangement assumed for the SAGs. For instance, this leads to increased values for the gravity-gradient torque, which excites more easily the spacecraft out of its reference attitude configuration. Still, it is clear that the viscoelastic damping strategy remains able to reduce control effort requirements as well as attitude disturbances, which is a critical requirement for satellites performing sensing/observation missions.

CONCLUDING REMARKS

In this work, the equations of motion necessary to analyze the attitude and vibration control of a satellite comprising a rigid hub and flexible elements, such as SAGs, have been put forward using FEs and Lagrangian mechanics. Attitude control was assumed to be accomplished by RWs driven by a PID feedback law. Vibration attenuation has been handled using viscoelastic materials, introduced in the form of springs interconnecting the SAGs' panels. The obtained results have shown that viscoelastic materials can be effective in dampening elastic responses in short intervals of time, and in alleviating the torques required by the ACS. Despite encouraging, attention needs to be taken into account for the selection of an adequate viscoelastic material that can handle the wide range of temperature variations to which spacecraft are subjected to, as well as the harsh space environment. Yet another inherent issue with the use of viscoelastic materials is owed to added weight. Of course, one should also remind that, being a passive vibration control strategy, the proposed approach should not destabilize the system nor require energy budget from the spacecraft to perform its role. Overall, viscoelastic materials look promising for the considered application.

ACKNOWLEDGMENTS

The authors are thankful for the continuous support of their research activities by the Brazilian agencies CNPq, CAPES and FAPESP.

REFERENCES

Bang, H., Ha, C.K. and Kim, J.H., 2005. "Flexible spacecraft attitude maneuver by application of sliding mode control". *Acta Astronautica*, Vol. 57, No. 11, pp. 841–850.

Bathe, K.J. and Baig, M.M.I., 2005. "On a composite implicit time integration procedure for nonlinear dynamics". *Computers & Structures*, Vol. 83, No. 31-32, pp. 2513–2524.

da Fonseca, I.M., Rade, D.A., Goes, L.C.S. and de Paula Sales, T., 2017. "Attitude and vibration control of a satellite containing flexible solar arrays by using reaction wheels, and piezoelectric transducers as sensors and actuators". *Acta Astronautica*, Vol. 139, pp. 357–366. ISSN 0094-5765.

Galucio, A.C., Deü, J.F. and Ohayon, R., 2004. "Finite element formulation of viscoelastic sandwich beams using fractional derivative operators". *Computational Mechanics*, Vol. 33, No. 4, pp. 282–291.

Modi, V.J., 1974. "Attitude dynamics of satellites with flexible appendages-a brief review". *Journal of Spacecraft and Rockets*, Vol. 11, No. 11, pp. 743–751.

Sales, T.P., Rade, D.A. and De Souza, L.C.G., 2013. "Passive vibration control of flexible spacecraft using shunted piezoelectric transducers". *Aerospace Science and Technology*, Vol. 29, No. 1, pp. 403–412.

Soovere, J. and Drake, M.L., 1985. "Aerospace structures technology damping design guide vol. 3". Technical report, AFWAL TR-84-3089, US Air Force, Wright-Patterson AFB, OH, USA.

TayyebTaher, M. and Esmaeilzadeh, S.M., 2017. "Model predictive control of attitude maneuver of a geostationary flexible satellite based on genetic algorithm". *Advances in Space Research*, Vol. 60, No. 1, pp. 57–64.

Wang, Z., Jia, Y., Xu, S. and Tang, L., 2016. "Active vibration suppression in flexible spacecraft with optical measurement". *Aerospace Science and Technology*, Vol. 55, pp. 49–56.

RESPONSIBILITY NOTICE

The authors are the only responsible for the printed material included in this paper.